Engineering in Life Sciences

WILEY-VCH

Engineering in Life Sciences

RESEARCH ARTICLE OPEN ACCESS

In Vivo Online Monitoring of Intracellular Lipid Accumulation in *Ustilago maydis*

Kira Müntjes[1,2] | Lesley Plücker[1,2] | Magnus Philipp[1,2] | Paul Richter[2,3] | Marcel Mann[2,3] | Michael Feldbrügge[1,2] | Kerstin Schipper[1,2]

[1]Institute of Microbiology, Heinrich-Heine University Düsseldorf, Düsseldorf, Germany | [2]Bioeconomy Science Center (BioSC), C/O Forschungszentrum Jülich, Jülich, Germany | [3]Chair of Biochemical Engineering, RWTH Aachen University, Aachen, Germany

Correspondence: Michael Feldbrügge (feldbrue@hhu.de) | Kerstin Schipper (kerstin.schipper@hhu.de)

Received: 1 October 2024 | **Revised:** 7 May 2025 | **Accepted:** 29 September 2025

Funding: The scientific activities of the Bioeconomy Science Center were financially supported by the Ministry of Culture and Science within the framework of the NRW Strategieprojekt BioSC (No. 313/323-400-002 13).

Keywords: fluorescence reporter | lipid droplets | online monitoring | single-cell oil | *Ustilago maydis*

ABSTRACT

Single cell oils produced in microorganisms constitute appealing alternatives to plant oils. Oleaginous fungi accumulate triacylglycerols in lipid droplets (LD). Their biosynthesis is typically induced under nitrogen limitation. We exploit the fungal model *Ustilago maydis* for oil production. The stain 4,4-difluoro-1,3,5,7,8-pentamethyl-4-bora-3a,4a-diaza-s-indacene (BODIPY) can be used to track LD formation during cultivation but this expensive compound is only affordable at small-scale. Therefore, mutant screening for optimization of oil production and composition would benefit from an inexpensive online monitoring system. Accordingly, we aimed at developing an intrinsic reporter that is suitable to track oil formation even in larger cultures. From three tested candidates, the potential delta(24)-sterol C-methyltransferase Erg6 turned out to be the best reporter. Fluorescence microscopy confirmed its localization at the LD membrane. After optimization, Erg6 fused to mKate2, expressed from a promoter derived from glycolipid biosynthesis, showed a good correlation of fluorescence with oil accumulation. Time course experiments in micro-cultivators demonstrated that the fluorescence read-out can be used to track oil formation starting at the onset of nitrogen limitation to approximate the LD amount. In essence, our study introduces a biosensor for oil monitoring that can easily be transferred to other oleaginous yeasts.

1 | Introduction

The demand for vegetable oils, in particular palm oil, is steadily increasing and is accompanied by negative ecological effects, especially concerning deforestation [1, 2]. Single-cell oils (SCO) derived from oleaginous microorganisms are considered promising alternatives to vegetable oils. These eukaryotic microbes store triacylglycerols (TAG) in the form of intracellular lipid droplets (LD), accumulating to more than 70% of the total biomass. LDs are known as ubiquitous dynamic organelles with essential functions in lipid homeostasis. They are derived from the endoplasmic reticulum (ER) and share a conserved structure throughout eukaryotes in which the hydrophobic core of neutral lipids is surrounded by a phospholipid monolayer with a limited number of associated proteins [3]. Excess oil deposition in LD is typically induced by nitrogen starvation, that is, with the complete use of the nitrogen source while carbon is still present in access [4]. While first SCOs are now being produced industrially,

Abbreviations: BODIPY, 4,4-difluoro-1,3,5,7,8-pentamethyl-4-bora-3a,4a-diaza-s-indacene; LD, lipid droplet; SCO, single cell oil; TAG, triacylglycerols.

Summary

- Microbial oils are promising, environmentally friendly alternatives to plant oils and have the potential of a huge market share once competitive production and isolation processes are accomplished.
- Online monitoring is key to efficient engineering of single cell oil producing microorganisms and bioprocess optimization in order to achieve competitive products.
- Here, we present an inexpensive, fluorescence-based reporter that can be used to track the approximate oil accumulation of microbial cultures in vivo. This omits the use of expensive dyes or offline methodology with a high workload.
- While we established the biosensor in the yeast form of the fungal microorganism *U. maydis*, the evolutionary conservation of the underlying protein Erg6 will allow for a straightforward transfer of the methodology to other oleaginous yeasts.

their exploitation is still limited by production volume and product diversity, resulting in prices that are not yet competitive to those of palm oil [5–8]. Thus, further research to optimize the production platforms and processes in terms of substrate use, oil titers, and oil composition is essential to yield competitive solutions. This requires intense genetic pathway engineering and high-throughput screening of cultivation or process conditions.

To date, the most commonly explored oleaginous microorganisms are yeasts, and genetic engineering has pushed forward the field tremendously. For instance, *Cutaneotrichosporon oleaginousus* is capable of accumulating up to 80% of its dry weight in lipids [9]. Due to its fast growth and broad substrate spectrum, it is considered a promising SCO production host from sustainable sources, such as for agro-industrial wastes [10]. The red yeast *Rhodotorula glutinis* is another example, synthesizing oil with a profile that might be suitable for the production of the so-called third-generation biodiesel. Furthermore, this yeast is known for its ability of carotenoid synthesis [11, 12]. Importantly, the prime example, *Yarrowia lipolytica* [13], has been engineered to secrete up to 85% of its fatty acids to facilitate downstream processing [14], and tailor-made synthesis of fatty acids with varying carbon chain lengths has been achieved [15]. Besides oleaginous yeasts, filamentous fungi such as *Aspergillus oryzae* [16] and microalgae like *Aurantiochytrium limacinum* [17] have also been reported to accumulate large amounts of SCO. This diversity allows for the production of a broad range of oils produced in different bioprocesses.

A great advantage in the production of SCOs in comparison to plant oils is the possibility to use renewable feed stocks obtained from waste streams. Specific examples include SCO production by *C. oleaginousus* based on the fermentation of lignocellulosic hydrolysate from paper mill waste streams, a process that reduces costs and carbon emissions compared to the use of glucose [18]. Engineered *Ashbya gossypii* was successfully employed for fermentation of hydrolyzed Eucalyptus bark supplemented with corn steep liquor, yielding an oil titer of 1.4 g/L [19].

Ustilago maydis is of increasing interest as a microbial production chassis and especially interesting as a host for SCO biosynthesis. While known as corn smut [20], this fungal model can be cultivated in an innocuous non-pathogenic, saprotrophic yeast form in the laboratory [21]. Strong arguments for using *U. maydis* for biotechnological purposes are its long-studied biology, the availability of a convenient toolset for efficient genetic manipulation as well as its very well annotated genome [22, 23]. In its yeast stage, *U. maydis* naturally produces biotechnologically relevant compounds, including organic acids, glycolipids, and SCO [23, 24]. In addition, heterologous sesquiterpenes and proteins were successfully synthesized [25–28]. Notably, *U. maydis* is also considered for biomass valorization since it grows on a variety of soluble sugars, including pentoses and biomass components [29–31].

As in other oleaginous organisms, oil formation in *U. maydis* is triggered by nitrogen starvation, and lipids are stored in LDs [24]. Interestingly, *U. maydis* cells lacking the biosynthesis of both glycolipids, mannosylerythritol lipids (MELs), and ustilagic acid show elevated SCO levels [32]. Hence, this strain is a promising precursor for optimizing yield and composition of the produced fatty acids. Tracking oil accumulation is key to an efficient pipeline for process optimization. Recently, the LD index assay has been introduced for quantification of neutral lipids in *U. maydis* [33]. This assay is based on lipid fluorescence recovery of the dye 4, 4-difluoro-1,3,5,7,8-pentamethyl-4-bora-3a,4a-diaza-s-indacene (BODIPY) 493/503, which is highly specific for neutral lipids under quenching conditions. More specifically, cells are sampled from a culture to be analyzed, fixed with formaldehyde, and finally mixed with a BODIPY solution quenched with potassium iodide [33]. Fluorescence is recovered for BODIPY associated with LD but not for the remaining dye. Importantly, in the LD index assay, samples of the cultures are analyzed offline, yielding accurate information on the oil content. Alternatively, BODIPY and other lipid dyes can also be used for online monitoring of cultures [34]. However, the prizing of these compounds is hindering their use in high-throughput methods or larger culture volumes.

In the present study, we have established and optimized an alternative online read-out to approximately monitor LD accumulation by fluorescent labeling of an LD-associated protein. This tool allows for the inexpensive and sustainable online tracking of cultures from microbioreactors, fluorescence readers or shake flasks up to bioreactor scale, given a fluorescence probe is available. It hence constitutes a valuable addition to the existing dyes and can be exploited to optimize oil production in this versatile microorganism, thereby speeding up the optimization of microbial oil production.

2 | Materials and Methods

2.1 | Accession Numbers

U. maydis gene and protein sequences are available from Uniprot (https://uniprot.org), with the following accession numbers: A0A0D1DTN0 (Sei1; UMAG_06049), A0A0D1CJH5 (Per1, UMAG_04910), and A0A0D1C4Q9 (Erg6, UMAG_03182).

2.2 | Molecular Cloning and Strain Generation

All strains used in this study were generated in the background of the oil producing strain MB215cyp1Δemt1Δ (DSM17147) (Table 1) [32, 35]. Modifications for oil detection via fluorescent proteins were conducted in the *ip* locus using integrative plasmids that mediate carboxin resistance [27]. Integrative plasmids (p123 derivatives) [36] were linearized within the *ip* gene for transformation, and the correct integration and the copy number of the inserted plasmids was verified by Southern blot analysis [27], using a probe hybridizing with the *ip* locus [27]. Details on plasmid generation and sequence maps are available upon request.

2.3 | Cultivation

During strain generation and for propagation, *U. maydis* strains were grown at 28°C in complete medium (CM) supplemented with 1% (w/v) glucose (CM-glc) [37]. Solid medium was supplemented with 2% (w/v) agar. CM-glc agar plates were used for streaking of all the strains. Modified Verduyn [38] medium was used for BioLector cultivations and microscopy, including all nitrogen-starvation experiments, and supplemented with 100 g/L glucose, as described before [32]. For nitrogen limitation, 0.5 g/L KH_2PO_4 and 1.6 g/L $(NH_4)_2SO_4$ were supplemented, while cultures without limitation were grown with 1.0 g/L KH_2PO_4 and 5 g/L $(NH_4)_2SO_4$. Both medium variants were buffered with 0.1 M MES buffer (pH 6.5).

A BioLector system (m2p-labs GmbH) equipped with 48-well round-well plates (M2P-MTP-R48-B) without optodes was used for all micro-cultivations with online monitoring. Precultures were inoculated in CM supplemented with 1% (w/v) glucose and grown overnight at 28°C with constant shaking (200 rpm) in test tubes. The next morning, 20 mL main cultures were inoculated (CM with 1 % glucose (w/v)) in unbaffled shake flasks, with a starting OD_{600} of 0.125 and grown at 28°C with constant shaking (200 rpm) till reaching an OD_{600} of 1. Subsequently, the cultures were washed once in 20 mL of sterile H_2O, and the respective amount of suspension was used to achieve an OD_{600} of 0.1 in 15 mL volume. The cells were centrifuged again and resuspended in 15 mL of Verduyn medium, either for nitrogen limiting conditions (1.6 g/L $(NH_4)_2SO_4$) or without limitation (5 g/L $(NH_4)_2SO_4$). From each suspension, 1.5 mL was transferred to round well plates. Optionally, BODIPY 493/503 (Thermo Fisher) was added at a concentration of 5 µM. Three channels were used to collect data: green fluorescent protein (Gfp) (Ex 488 nm/Em 520 nm, gain 40) to detect BODIPY, Rfp (gain 80) to detect mKate2 fluorescence, and Backscatter (gain 15) to track cell growth in the BioLector. The experiment was performed in biological triplicates, with each measurement comprising three technical replicates. The cell density as well as the fluorescence signal were determined every 30 min for a total time of 60 to 140 h at constant conditions of 28°C and 1000 rpm. For data analysis, the mean value of technical replicates for each time point and in each measurement was calculated. The background reads of the respective medium (with or without BODIPY) were subtracted from these values.

2.4 | Western Blot Analysis

To analyze the biosensor synthesis, total protein was prepared from cells of the indicated growth stages. To this end, 20 mL cultures were harvested by centrifugation (8000 rpm, 15 min, 4°C). Cell pellets were washed in 4 mL of chilled PBS once and centrifuged again (13,000 rpm, 10 min, 4°C). After removing the cell-free supernatant, cells were disrupted using a Retsch Mill (3× 30 Hz, 30 s each). Next, the pellets were resuspended in 0.5 mL of denaturing lysis buffer (100 mM sodium phosphate buffer pH 8.0, 10 mM Tris/HCl pH 8.0, 8 M urea, 1 mM DTT, 1 mM PMSF, 2.5 mM benzamidine, 1× complete protease inhibitor cocktail [Roche]) using a Vibrax (800 rpm, 5 min), and cell debris was removed by centrifugation (13,000 rpm, 10 min, 4°C). The supernatant was used for standard protein determination using Bradford reagent (BioRad, Hercules, CA, United States). A total of 10 µg of total protein was separated on Bolt 4%–12% Bis-Tris Plus (Invitrogen) gradient gels and transferred to a nylon membrane (Amersham, hybond-P) using semi-dry Western blotting. Gfp-tagged protein was detected using primary mouse anti-Gfp antibodies (1:1000; Millipore/Sigma), and a secondary anti-mouse IgG horseradish peroxidase (HRP) conjugate (1:4000 Promega) was used as a secondary antibody. For actin detection, primary mouse anti-actin antibodies (1:1000) were applied. HRP activity was then detected using the Amersham ECL Primer Western Blotting Detection Reagent (GE, Healthcare) and a gel imager (Amersham ImageQuant 800).

2.5 | Microscopy and Image Processing

Microscopical analyses were conducted using a Zeiss Axio Observer.Z1 equipped with a BSI express camera (Teledyne Potometrics, Tucson, AZ, USA) and a VS-LMS4 Laser-Merge-System (Visitron Systems, Puchheim, Germany) that combines solid-state lasers for excitation of Gfp (488 nm at 50 or 100 mW) and Rfp/mKate2 (561 nm at 50 or 150 mW). To evaluate the individual reporter strains, yeast cells were first cultivated in a preculture (CM with 1% glucose (w/v)) followed by a main culture of 20 mL of Verduyn medium for nitrogen limiting conditions (1.6 g/L $(NH_4)_2SO_4$; start OD_{600} 0.5). The cultures were incubated for a total of 72 h at 28°C and 200 rpm in baffled flaks with loose lids. After 24, 48, and 72 h, the formation of oil droplets was analyzed using differential interference contrast microscopy (DIC) at 40× magnification. The localization of the individual proteins (Per1, Erg6, Sei1) fused to enhanced green fluorescent protein (eGfp) or mKate2 was analyzed using laser-based epifluorescence microscopy. The same setup was used to analyze the strength of expression of Erg6-Gfp using different promoters. The progenitor strain MB215cyp1Δemt1Δ, which shows enhanced oil formation but does not carry fluorescence proteins, served as a control in each case. Here, the oil droplets were stained using BODIPY. In the strains in which Erg6 is expressed in fusion to mKate2, co-localization studies of both the mKate2 and BODIPY signals were performed. All images were processed and analyzed using Metamorph software (version 7.7.0.0, Molecular Devices, Seattle, IL, USA). Gfp and BODIPY signals are shown in green, mKate2 signals in magenta. Overlays were generated to better illustrate the co-localization of two fluorescence signals (BODIPY and mKate2). Co-localization is depicted in white. Quantification of lipid droplets was done using the ImageJ plugin Cell Counter

TABLE 1 | Strains used in this study.

Strain	Internal strain collection number	Parental strain	Vector	Genotype	Reference
MB215	UMa1160	—	—	Wildtype strain (mating type *a2b13*)	DSM17144
MB215Δcyp1Δemt1	UMa2112	MB215	—	*emt1*Δ (HygR), c*yp1Δ* (NatR)	DSM 17147; [35]
MB215Δcyp1Δemt1/P_{mtt1}Per1-Gfp	Ux53	UMa2112	p123_Pmtt1_per1-egfp_cbxR (pUX0079)	*emt1*Δ (HygR), c*yp1Δ* (NatR) *ip*^{S} P_{mtt1}::04910::gfp *ip*^{R} (CbxR)	This work.
MB215Δcyp1Δemt1/P_{mtt1}Erg6-Gfp	Ux54	UMa2112	p123_Pmtt1_erg6-egfp_cbxR (pUX0081)	*emt1*Δ (HygR), c*yp1Δ* (NatR) *ip*^{S} P_{mtt1}::03182 ::gfp *ip*^{R} (CbxR)	This work.
MB215Δcyp1Δemt1/P_{mtt1}Sei1-Gfp	Ux55	UMa2112	p123_Pmtt1_sei1-egfp_cbxR (pUX0080)	*emt1*Δ (HygR), c*yp1Δ* (NatR) *ip*^{S} P_{mtt1}::umag_06049::gfp *ip*^{R} (CbxR)	This work.
MB215Δcyp1Δemt1/P_{cyp1}Erg6-Gfp	Ux81	UMa2112	p123_ Pcyp1_erg6-egfp_cbxR (pUX0082)	*emt1*Δ (HygR), c*yp1Δ* (NatR) *ip*^{S} P_{cyp1}::umag_03182 ::gfp *ip*^{R} (CbxR)	This work.
MB215Δcyp1Δemt1/P_{cyp2}Erg6-Gfp	Ux82	UMa2112	p123_ Pcyp2_erg6-egfp_cbxR (pUX120)	*emt1*Δ (HygR), c*yp1Δ* (NatR) *ip*^{S} P_{cyp2}::umag_03182 ::gfp *ip*^{R} (CbxR)	This work.
MB215Δcyp1Δemt1/P_{emt1}Erg6-Gfp	Ux83	UMa2112	p123_ Pemt1_erg6-egfp_cbxR (pUX121)	*emt1*Δ (HygR), c*yp1Δ* (NatR) *ip*^{S} P_{emt1}::umag_03182 ::gfp *ip*^{R} (CbxR)	This work.
MB215Δcyp1Δemt1/P_{emt1}Erg6-Kat	Ux143[a]	UMa2112	p123_ Pemt1_Erg6-mKate2_cbxR (pUX195)	*emt1*Δ (HygR), *cyp1*Δ (NatR) *ip*^{S} P_{emt1}::umag_03182::mKate2 *ip*^{R} (CbxR)	This work.

Note: UMAG_06049, annotated seipin; UMAG_04910, predicted perilipin; UMAG_03182, predicted Erg6 homolog; UMAG_05079, Mtt1 - cis-aconitate exporter; Kat, mKate2.

[a]Different variants of this strain are available, harboring 1 (1x), 2 (2x), or multiple copies (nx, exact copy number has not been determined) of the *ip* insertion plasmid.

[39]. The average amount of LD's/cell was calculated from at least 500 cells/strain.

3 | Results and Discussion

3.1 | Identification of a LD Reporter Candidate

In order to identify a suitable reporter for LD formation, we conducted a candidate approach and tested three different proteins potentially localizing to LDs or to its surrounding membrane (Figure 1A; Figure S1): (i) Sei1 (UMAG_06049), a protein annotated as seipin in the uniprot database (A0A0D1DTN0_USTMA) and potentially involved in LD assembly [40]; (ii) Per1 (UMAG_04910), a putative perilipin that had been identified in a proteomic analysis of LDs [24]; and (iii) Erg6 (UMAG_03182), a conserved protein homologous to delta(24)-sterol C-methyltransferases that converts zymosterol to fecosterol in the ergosterol biosynthetic pathway [41] (54% and 31% amino acid identity to Erg6 from *Saccharomyces cerevisiae* and COQ3 from *Homo sapiens*, respectively; Figure S1). First, to investigate if these proteins indeed localize to LDs, we used homologous recombination to insert constructs for expression of the individual proteins fused to the eGfp in the background of the oil production strain *U. maydis* MB215Δemt1Δcyp1 [32, 35] (Figure 1A). Of note, this strain still contained the original copies of all genes to minimize the disturbance of the cell metabolism. Constitutive expression of the proteins might lead to undesired side-effects due to the absence of their natural target organelle. To thus ensure the expression of the constructs during nitrogen starvation when LD accumulate, we aimed on conditionally linking the expression of the candidates to LD accumulation and hooked up the genes to the promoter region of *mtt1*. This gene encodes a mitochondrial cis-aconitate exporter and is part of the itaconic acid biosynthesis gene cluster induced at nitrogen limiting conditions [42]. Western blot analyses showed that only the Erg6 fusion proteins were produced at full length and without significant degradation at nitrogen limiting conditions. While Per1-Gfp showed a strong degradation band at the size of free Gfp instead of full-length fusion protein, no clear signal was detected for Sei1-Gfp (Figure 1B). Next, to evaluate protein localization, we cultivated the strains in liquid culture and conducted fluorescence microscopy along a 3 day-time course. For these experiments, we used a medium with a carbon-nitrogen ratio that leads to nitrogen limitation in the culture starting at approximately 30 h post inoculation. Control cells stained with BODIPY confirmed the presence of small LD at Day 1 and larger droplets at Days 2 and 3 (Figure 1C). We detected Gfp fluorescence in all three strains producing biosensor candidates. Erg6-Gfp showed the expected LD membrane localization during nitrogen limitation, confirming earlier studies that used the protein for visualization of LDs in *U. maydis* hyphae [41]. By contrast and in accordance with the Western blot analysis, the fluorescence signal was mostly cytoplasmatic for Per1-Gfp, indicating the detection of residual free Gfp instead of the fusion protein. Sei1-Gfp fluorescence was very weak and also not clearly associated with LDs, confirming its low production level (Figure 1C). In conclusion, we identified Erg6 as the best suited biosensor candidate for online read-out. However, the overall fluorescence, while clearly visible during microscopy, was not strong enough for a quantitative readout, that is, during online monitoring, even at a stage of the cultures where we observed large LDs.

3.2 | Finetuning of Biosensor Expression

Due to the fact that *U. maydis* yeast cells show significant Gfp background signal and the fluorescence signal of Erg6-Gfp was not very bright (Figure 1C), we next aimed for optimizing the expression of the biosensor. To this end, we chose three alternative sequence stretches derived from the promoter regions of genes from glycolipid biosynthesis (P_{cyp1}, P_{cyp2}, and P_{emt1}), that are known to be induced at nitrogen limiting conditions and generated translational fusions with *erg6* (Figure 2A). While *cyp1* and *cyp2* code for P450 monooxygenases involved in ustilagic acid biosynthesis [43], *emt1* encodes a glycosyltransferase, catalyzing the first step of mannosylerythritol biosynthesis [44]. A fluorescence microscopy time-course revealed that the strain with the P_{cyp1} expression cassette showed strong Gfp fluorescence in the LD membranes. However, some cells that clearly contained LDs completely lacked a Gfp signal, suggesting that there is a strong population heterogeneity potentially caused by regulatory issues at the level of protein stability or post-translational modifications. The two other strains had homogenous green fluorescent LD membranes, but the signal was stronger and had a better signal/noise ratio in the strain containing P_{emt1} (Figure 2B). Notably, the nature of the fluorescence signal varied between 1 and 2 days post inoculation of the culture, in that it first emerged in rather compact spots and only later on clearly labeled LD membranes. As LD biogenesis occurs at distinct sites in the ER, it is conceivable that these sites are labeled after 1 day, while later on, the LD are fully assembled, and thus the Erg6 signal is then apparent in the membrane [45]. Alternatively, the diameter of the LDs in the early stage of cultivation is simply too small to resolve the vesicular structure microscopically. In essence, the *emt1* promoter turned out to be the best suited promoter for tracking LD accumulation.

3.3 | Reduction of Background Fluorescence for Biosensor Optimization

As mentioned above, *U. maydis* yeast cells show significant cytoplasmic background fluorescence in the Gfp emission range (Figures 1A and 2A). Hence, we next tested if a fusion of Erg6 to mKate2, which is a very bright and stable red-emitting variant of mCherry [46], shows improved features for oil online monitoring as they have different excitation and emission ranges. Therefore, we generated strains carrying transcriptional fusions of Erg6 with mKate2 (MB215P_{emt1}Erg6Kat; Figure 3A). Importantly, the insertion locus used for homologous recombination supports the selection of mutants with single, double, or multiple insertions of the expression cassette, allowing to screen for the optimal expression strength for LD monitoring. Again, we performed a microscopic time-course over 3 days, with the different mutants. Importantly, the use of mKate2 as a fluorescence reporter now also enabled counter staining using BODIPY to visualize the LDs (Figure 3B). Microscopic inspection confirmed that the fusion protein Erg6-Kat also localized to the LD membranes, surrounding the BODIPY stained lipids (see overlays of both channels). Importantly, cytoplasmic background fluorescence

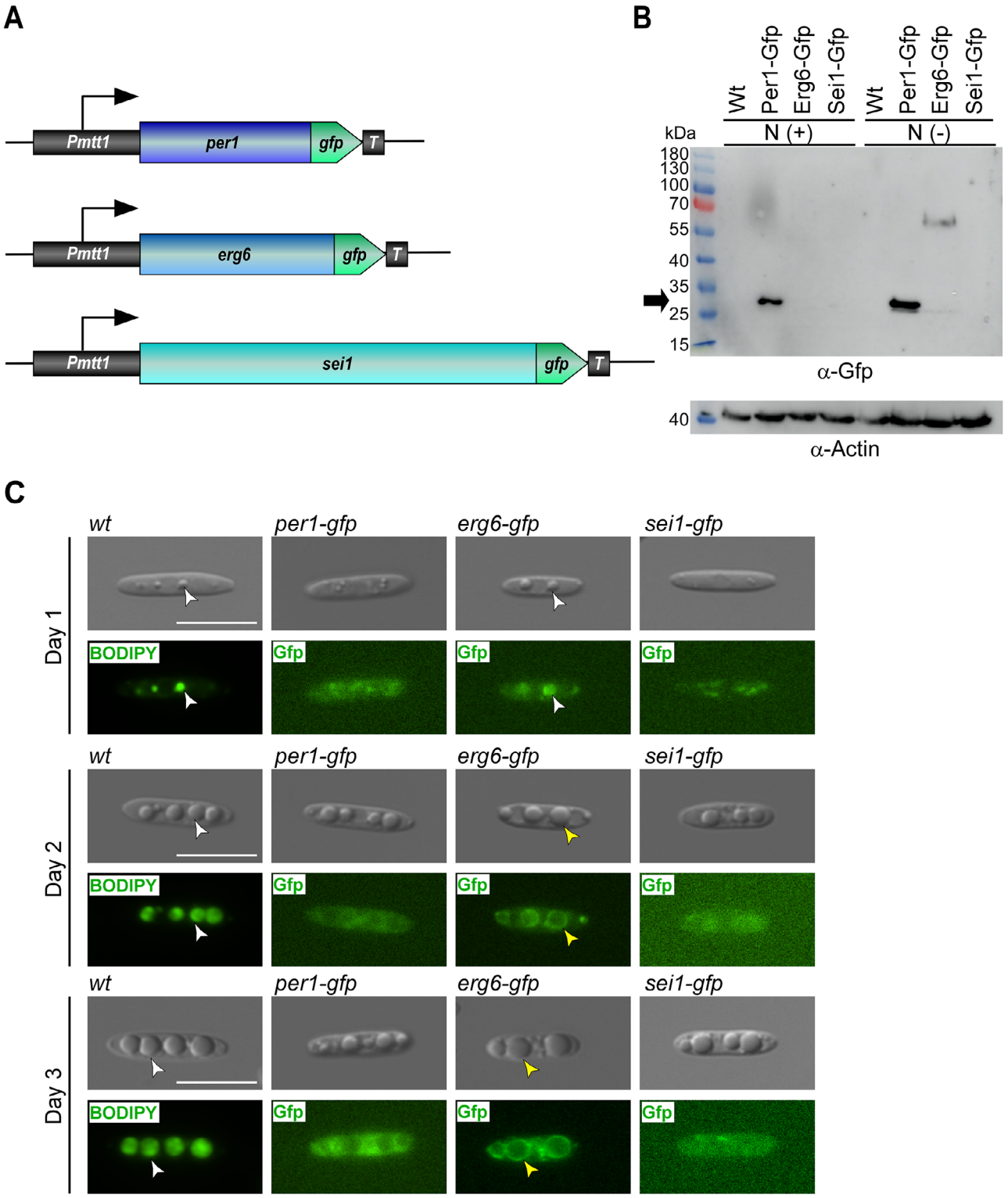

FIGURE 1 | Characterization of candidates for LD monitoring. (A) Schematic drawing of genetic constructs for expression of candidate proteins. All genes were generated as in-frame fusions to *gfp*. P_{mtt1} corresponds to the promoter region of the *mtt1* gene (umag_05079), encoding mitochondrial tricarboxylate transporter 1, Mtt1. T, nos terminator. (B) Western blot analysis to detect the production of the candidates at conditions with sufficient nitrogen (N(+)) and at nitrogen limitation (N(−)). Proteins were detected with an anti-Gfp antibody. Putative free Gfp resulting from degradation is marked with an arrow. Expected protein sizes: Per1-Gfp (60 kDa), Erg6-Gfp (65 kDa), Sei1 (107 kDa). Actin was used as a loading control (41 kDa) detected after a washing step on the identical membrane. Wt, progenitor strain MB215Δcyp1Δemt1. (C) Microscopic visualization of protein localization during nitrogen-starvation phase (24–72 h post inoculation). BODIPY was used to visualize LDs. Wt, progenitor strain MB215Δcyp1Δemt1. White arrowheads depict fluorescence within LD while yellow arrowheads show fluorescing LD membranes. Magnification: 40×; scale bars, 10 μm.

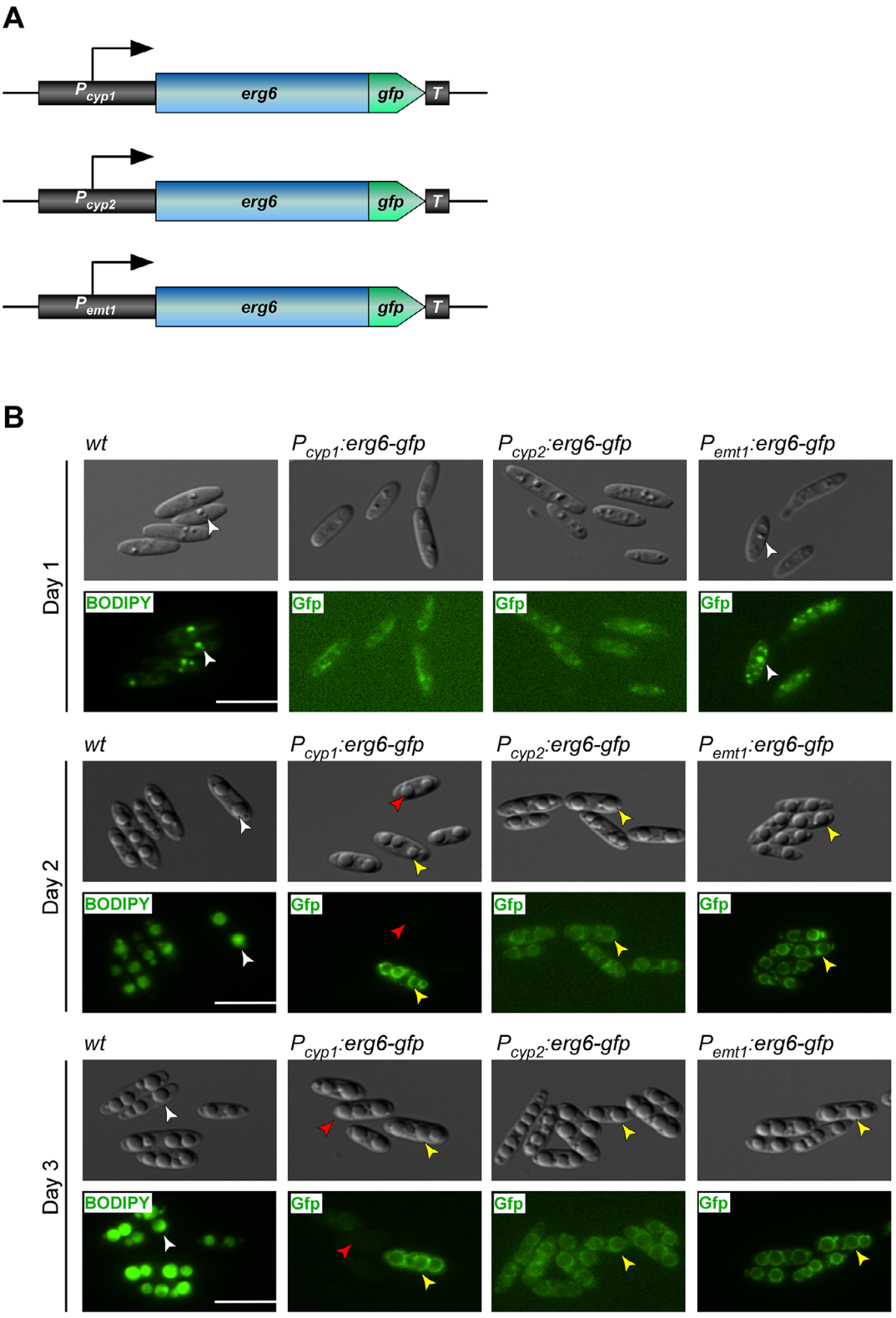

FIGURE 2 | Comparative Erg6-Gfp visualization using different nitrogen starvation-induced promoters for gene expression. (A) Schematic drawing of expression constructs. All genes were generated as in-frame fusions to *gfp*. P_{xx} corresponds to the promoter region of the indicated nitrogen starvation-induced genes from the MEL and UA gene clusters. T, nos terminator. (B) Fluorescence microscopic visualization of Erg6-Gfp expressed from indicated genetic constructs. Nitrogen starvation was reached about 2 days post inoculation. BODIPY was used to visualize LDs. Wt, progenitor strain MB215Δcyp1Δemt1. White arrowheads depict fluorescence within LD while yellow arrowheads show fluorescing LD membranes. Red arrowheads depict cells that lack a biosensor signal, indicating population heterogeneity. Note the overall high intracellular background in the Gfp channel. Magnification: 40×; scale bars, 10 μm.

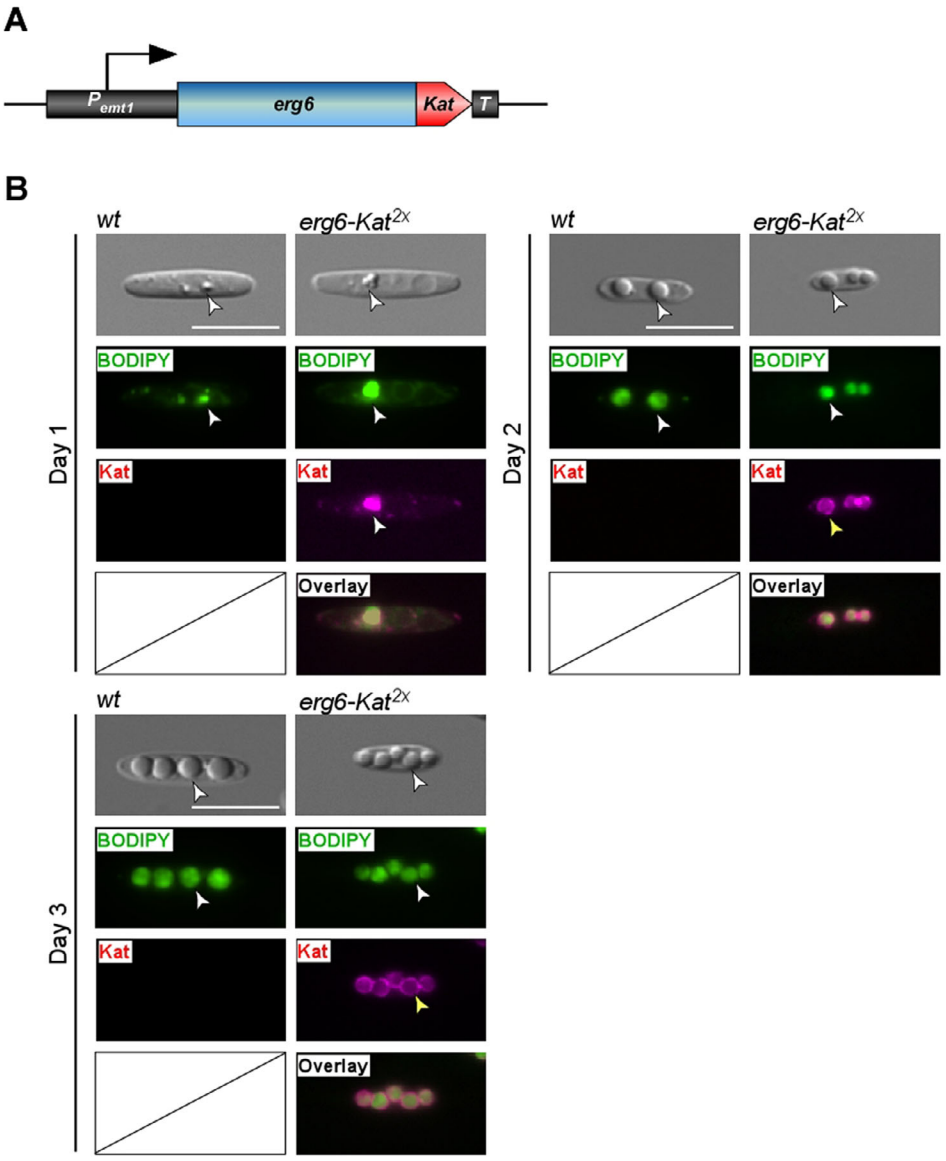

FIGURE 3 | Microscopic characterization of the optimized Erg6-Kat^{2x} biosensor strain harboring two copies of the expression construct. (A) Schematic drawing of expression construct for Erg6-Kat. P_{emt1} corresponds to the *emt1* promoter region. T, nos terminator. (B) Fluorescence microscopic visualization of Erg6-Kat expressed from the indicated genetic constructs. BODIPY staining was used to visualize LDs. Wt, progenitor strain MB215Δcyp1Δemt1. White arrowheads depict fluorescence within LD while yellow arrowheads show fluorescing LD membranes. 2×, expression construct inserted twice. Magnification: 40×; scale bars, 10 μm.

was now minimized. While a single insertion of the construct led to weaker fluorescence, the double insertion showed clear signals delimiting the green BODIPY fluorescence of the LDs (Figure 3B; Figure S2). The same was true for a mutant that carried multiple copies of the insertion construct. However, here we recognized that the number of LDs was strongly increased, pointing towards an effect of Erg6 overexpression on LD formation (Figures S2 and S3). In summary, the double inserted construct led to the best LD visualization with a low signal to noise ratio.

3.4 | In Vivo Monitoring With the Optimized Biosensor Erg6-Kat^{2x}

For an efficient screening of mutations, an online monitoring system would be very useful. Therefore, we used a BioLector micro-cultivation device to characterize the Erg6-Kat^{2x} reporter strain at nitrogen limiting conditions. As a control, we used the oil production strain MB215Δemt1Δcyp1 lacking the reporter construct. BODIPY staining was used to detect LD formation with the established methodology. Although backscatter detection is not reliable due to the presence of high oil concentrations, the data indicate that the cultures start to grow exponentially at about 15 h post inoculation (Figure S4). The continuous detection of green (BODIPY) fluorescence in the cultures showed that the signal started to increase at about 30–35 h post inoculation, marking the beginning of nitrogen limitation and thus, the onset of LD formation (Figure 4A). During the cultivation, BODIPY fluorescence then progressed with a steep increase and continued to increase weakly over the rest of the cultivation from about 75 h post inoculation (Figure 4A; Figure S4). Interestingly, red Erg6-Kat^{2x} fluorescence started to increase at the same time point, indicating that the detection of LDs at the onset of the nitrogen

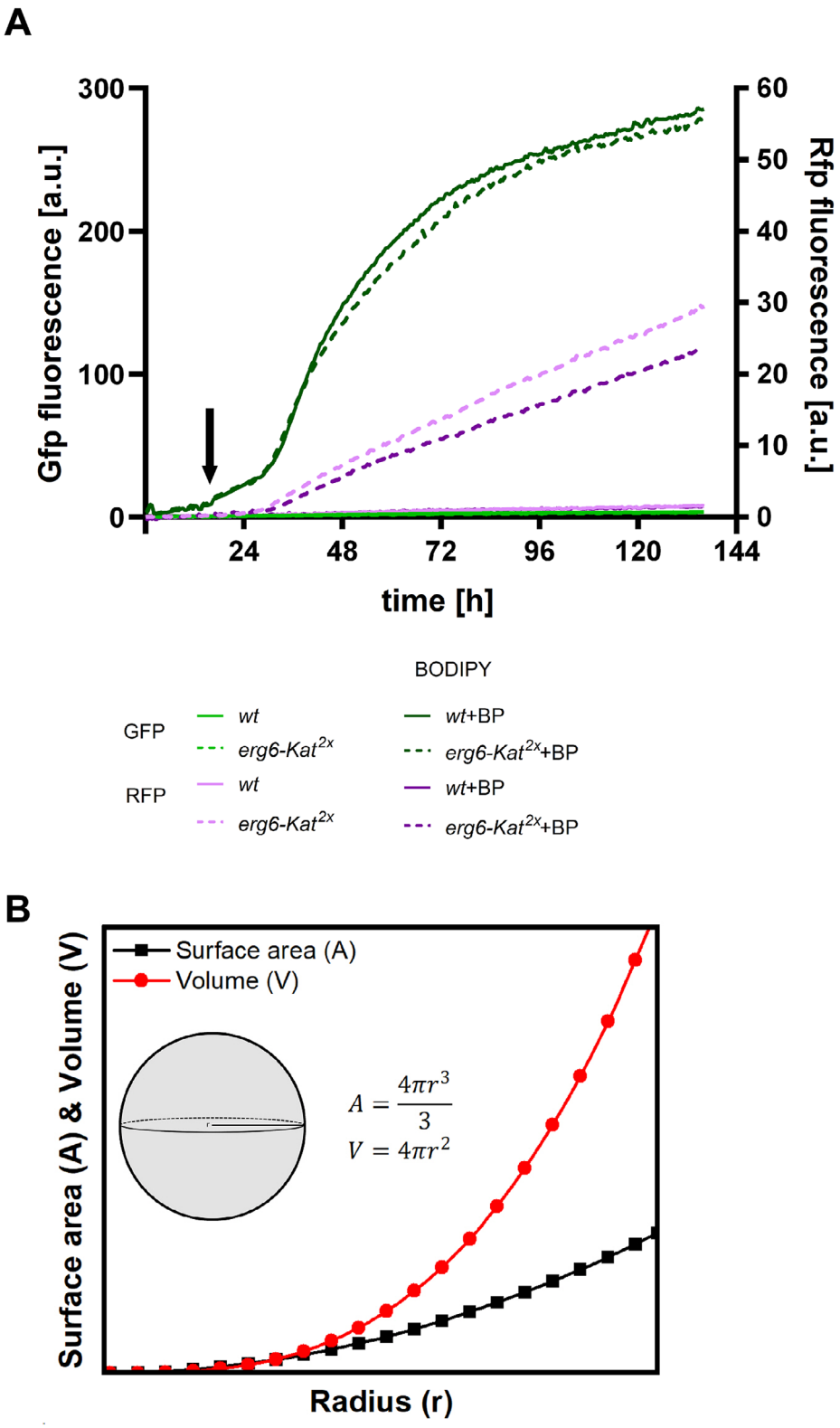

FIGURE 4 | In vivo monitoring of LD accumulation using Erg6K^{2x}. (A) Microscale cultivation in a BioLector device with parallel BODIPY staining. The onset of the exponential growth phase, as indicated by backscatter detection (Figure S3A) is indicated by an arrow. Replicate 1 is shown as a representative result of three biological replicates. See Figure S3 for additional data including biomass reads (backscatter). Gfp fluorescence of the samples is plotted on the left *Y*-axis in variants of green, while Rfp fluorescence of the same samples is plotted on the right *Y*-axis in variants of magenta. a.u., artificial units. The progenitor strain lacking the reporter (MB215Δemt1Δcyp1) was used as a control (wt). Values for samples without BODIPY are depicted in light green/magenta, values for samples including BODIPY are shown in dark green/magenta. Standard deviation is shown for backscatter reads (right panel). (B) Schematic representation of the change in surface area and volume for a sphere with a linearly increasing radius.

limitation phase is working. The fluorescence read-out then followed a linear increase, in contrast to the rather exponential increase of BODIPY fluorescence. This can be explained by the fact that BODIPY stains the entire droplet (a sphere), while Erg6-Kat labels the LD membranes from the outside, and thus only the surface of the LD is fluorescent. While the surface area of the sphere has a squared dependence on the radius, the volume has a cubic one. This interdependence of radius, surface area, and volume offers an explanation for the discrepancies observed between the two staining methods (Figure 4B). In essence, the Erg6-Kat^{2x} reporter is a suitable tool to track and approximate the amount of LD during cultivation.

4 | Concluding Remarks

To the best of our knowledge, we have developed the first fluorescent reporter that can be exploited to track LD formation not only microscopically as demonstrated before [41, 47, 48], but also in micro-cultivations by online monitoring red fluorescence. This will enable the screening of multiple strains with respect to oil formation, that is, in the framework of a genetic screen, medium and process optimization, or using reverse genetic approaches. While BODIPY could also be used for these applications, depending on the local supplier, the dye can be very expensive (e.g., about 2.50€ per 50 mL culture, Thermo Fisher), making our method a cost-effective and sustainable alternative. The strong evolutionary conservation of Erg6 (Figure S1) suggests that this strategy can likely be expanded to other organisms, ranging from fungi to even mammalian systems. We hypothesize that the biosensor can also be applied in larger culture volumes and even in fermentations, given that a fluorescence probe is available in the cultivation device [49, 50; https://www.scientificbio.com/multiparameter-sensor-for-shake-flasks]. In essence, we have provided a powerful and inexpensive alternative approach to track LD formation in liquid culture, given that the used organism can be genetically modified.

Acknowledgments

We thank our collaboration partners Dr. Guadalupe Guerra-Sánchez and Dr. Minerva Georgina Araiza Villanueva for valuable discussion about lipid droplet biology in *U. maydis*. We are particularly grateful to Theresa Heidrich, Simone Krüger, and Bettina Axler for excellent technical support as well as Dr. Florian Altegoer for critical reading of the manuscript. To ensure data FAIRness, we utilized the DataPLANT personal assistance network and its tool stack, centered around the DataHUB. We kindly acknowledge support by Sabrina Zander that was essential for generation of the annotated research context (ARC). The scientific activities of the Bioeconomy Science Center were financially supported by the Ministry of Culture and Science within the framework of the NRW Strategieprojekt BioSC (No. 313/323-400-002 13).

Open access funding enabled and organized by Projekt DEAL.

Conflicts of Interest

The authors declare no conflicts of interest.

Data Availability Statement

Data of the present study are included in the published article and its supplementary information. Further data, including the corresponding raw data, is available in the Data Hub [51] https://archive.nfdi4plants.org/records/5cw69-mt578. Our FAIR data publication can be found under DOI: https://doi.org/10.60534/5cw69-mt578.

References

1. E. Meijaard, T. M. Brooks, and K. M. Carlson, et al., "The Environmental Impacts of Palm Oil in Context," *Nature Plants* 6, no. 12 (2020): 1418–1426, https://doi.org/10.1038/s41477-020-00813-w.

2. A. Kumar, A. Sharma, and K. C. Upadhyaya, "Vegetable Oil: Nutritional and Industrial Perspective," *Current Genomics* 17, no. 3 (2016): 230–240, https://doi.org/10.2174/1389202917666160202220107.

3. J. A. Olzmann and P. Carvalho, "Dynamics and Functions of Lipid Droplets," *Nature Reviews Molecular Cell Biology* 20, no. 3 (2019): 137–155, https://doi.org/10.1038/s41580-018-0085-z.

4. C. Ratledge, "Regulation of Lipid Accumulation in Oleaginous Micro-Organisms," *Biochemical Society Transactions* 30 (2002): 1047–1050, https://doi.org/10.1042/bst0301047.

5. S. Parsons, C. J. Chuck, and M. C. McManus, "Microbial Lipids: Progress in Life Cycle Assessment (LCA) and Future Outlook of Heterotrophic Algae and Yeast-Derived Oils," *Journal of Cleaner Production* 172 (2018): 661–672, https://doi.org/10.1016/j.jclepro.2017.10.014.

6. K. T. Tan, K. T. Lee, A. R. Mohamed, and S. Bhatia, "Palm Oil: Addressing Issues and Towards Sustainable Development," *Renewable and Sustainable Energy Reviews* 13, no. 2 (2009): 420–427, https://doi.org/10.1016/j.rser.2007.10.001.

7. B. Wicke, R. Sikkema, V. Dornburg, and A. Faaij, "Exploring Land Use Changes and the Role of Palm Oil Production in Indonesia and Malaysia," *Land Use Policy* 28, no. 1 (2011): 193–206, https://doi.org/10.1016/j.landusepol.2010.06.001.

8. J. H. Schmidt, "Life Cycle Assessment of Five Vegetable Oils," *Journal of Cleaner Production* 87 (2015): 130–138, https://doi.org/10.1016/j.jclepro.2014.10.011.

9. N. I. Stellner, Z. S. Rerop, N. Mehlmer, M. Masri, M. Ringel, and T. B. Brück, "Expanding the Genetic Toolbox for *Cutaneotrichosporon oleaginosus* Employing Newly Identified Promoters and a Novel Antibiotic Resistance Marker," *BMC Biotechnology* 23, no. 1 (2023): 40, https://doi.org/10.1186/s12896-023-00812-7.

10. N. Di Fidio, F. Minonne, C. Antonetti, A. Maria, and R. Galletti, "*Cutaneotrichosporon Oleaginosus*: A Versatile Whole-Cell Biocatalyst for the Production of Single-Cell Oil From Agro-Industrial Wastes," *Catalysts* 11, no. 11 (2021): 1291.

11. A. M. Kot, S. Błażejak, A. Kurcz, I. Gientka, and M. Kieliszek, "Rhodotorula Glutinis—Potential Source of Lipids, Carotenoids, and Enzymes for Use in Industries," *Applied Microbiology and Biotechnology* 100, no. 14 (2016): 6103–6117, https://doi.org/10.1007/s00253-016-7611-8.

12. E. E. Karamerou, C. Theodoropoulos, and C. Webb, "A Biorefinery Approach to Microbial Oil Production From Glycerol by *Rhodotorula glutinis*," *Biomass and Bioenergy* 89 (2016): 113–122, https://doi.org/10.1016/j.biombioe.2016.01.007.

13. A. Beopoulos, J. Cescut, R. Haddouche, J.-L. Uribelarrea, C. Molina-Jouve, and J.-M. Nicaud, "*Yarrowia Lipolytica* as a Model for Bio-Oil Production," *Progress in Lipid Research* 48, no. 6 (2009): 375–387, https://doi.org/10.1016/j.plipres.2009.08.005.

14. R. Ledesma-Amaro, R. Dulermo, X. Niehus, and J.-M. Nicaud, "Combining Metabolic Engineering and Process Optimization to Improve Production and Secretion of Fatty Acids," *Metabolic Engineering* 38 (2016): 38–46, https://doi.org/10.1016/j.ymben.2016.06.004.

15. K. Wang, T.-Q. Shi, L. Lin, P. Wei, R. Ledesma-Amaro, and X.-J. Ji, "Engineering *Yarrowia lipolytica* to Produce Tailored Chain-Length Fatty Acids and Their Derivatives," *ACS Synthetic Biology* 11, no. 8 (2022): 2564–2577, https://doi.org/10.1021/acssynbio.2c00305.

16. L. Hui, C. Wan, D. Hai-Tao, C. Xue-Jiao, Z. Qi-Fa, and Z. Yu-Hua, "Direct Microbial Conversion of Wheat Straw Into Lipid by a Cellulolytic Fungus of *Aspergillus Oryzae* A-4 in Solid-State Fermentation,"

Bioresource Technology 101, no. 19 (2010): 7556–7562, https://doi.org/10.1016/j.biortech.2010.04.027.

17. T. Y. Huang, W. C. Lu, and I. M. Chu, "A Fermentation Strategy for Producing Docosahexaenoic Acid in *Aurantiochytrium Limacinum* SR21 and Increasing C22:6 Proportions in Total Fatty Acid," *Bioresource Technology* 123 (2012): 8–14, https://doi.org/10.1016/j.biortech.2012.07.068.

18. Z. S. Rerop, N. I. Stellner, and P. Graban, et al., "Bioconversion of a Lignocellulosic Hydrolysate to Single Cell Oil for Biofuel Production in a Cost-Efficient Fermentation Process," *Fermentation* 9 (2023): 189, https://doi.org/10.3390/fermentation9020189.

19. M. Francisco, T. Q. Aguiar, G. Abreu, S. Marques, F. Gírio, and L. Domingues, "Single-Cell Oil Production by Engineered *Ashbya Gossypii* From Non-Detoxified Lignocellulosic Biomass Hydrolysate," *Fermentation* 9, no. 9 (2023): 791, https://doi.org/10.3390/fermentation9090791.

20. A. Djamei, "Ustilago Maydis," *Current Biology* 33, no. 11 (2023): R458–R460, https://doi.org/10.1016/j.cub.2023.02.069.

21. M. Feldbrügge, R. Kellner, and K. Schipper, "The Biotechnological Use and Potential of Plant Pathogenic Smut Fungi," *Applied Microbiology and Biotechnology* 97, no. 8 (2013): 3253–3265, https://doi.org/10.1007/s00253-013-4777-1.

22. D. R. Olicón-Hernández, M. G. Araiza-Villanueva, J. P. Pardo, E. Aranda, and G. Guerra-Sánchez, "New Insights of *Ustilago Maydis* as Yeast Model for Genetic and Biotechnological Research: A Review," *Current Microbiology* 76, no. 8 (2019): 917–926.

23. N. Wierckx, K. Miebach, N. Ihling, K. P. Hussnaetter, J. Büchs, and K. Schipper, "Perspectives for the Application of Ustilaginaceae as Biotech Cell Factories," *Essays in Biochemistry* 65, no. 2 (2021): 365–379.

24. L. R. Aguilar, J. P. Pardo, M. M. Lomelí, O. I. L. Bocardo, M. A. Juárez Oropeza, and G. Guerra Sánchez, "Lipid Droplets Accumulation and Other Biochemical Changes Induced in the Fungal Pathogen *Ustilago maydis* Under Nitrogen-Starvation," *Archives of Microbiology* 199, no. 8 (2017): 1195–1209, https://doi.org/10.1007/s00203-017-1388-8.

25. J. Lee, F. Hilgers, A. Loeschke, K.-E. Jaeger, and M. Feldbrügge, "*Ustilago Maydis* Serves as a Novel Production Host for the Synthesis of Plant and Fungal Sesquiterpenoids," *Frontiers in Microbiology* 11 (2020): 1655, https://doi.org/10.3389/fmicb.2020.01655.

26. P. Sarkari, M. Reindl, and J. Stock, et al., "Improved Expression of Single-Chain Antibodies in *Ustilago maydis*," *Journal of Biotechnology* 191 (2014): 165–175, https://doi.org/10.1016/j.jbiotec.2014.06.028.

27. J. Stock, P. Sarkari, S. Kreibich, T. Brefort, M. Feldbrügge, and K. Schipper, "Applying Unconventional Secretion of the Endochitinase Cts1 to Export Heterologous Proteins in *Ustilago maydis*," *Journal of Biotechnology* 161, no. 2 (2012): 80–91, https://doi.org/10.1016/j.jbiotec.2012.03.004.

28. M. Terfrüchte, S. Wewetzer, and P. Sarkari, et al., "Tackling Destructive Proteolysis of Unconventionally Secreted Heterologous Proteins in *Ustilago maydis*," *Journal of Biotechnology* 284 (2018): 37–51, https://doi.org/10.1016/j.jbiotec.2018.07.035.

29. P. Stoffels, M. J. Müller, and S. Stachurski, et al., "Complementing the Intrinsic Repertoire of *Ustilago maydis* for Degradation of the Pectin Backbone Polygalacturonic Acid," *Journal of Biotechnology* 307 (2020): 148–163, https://doi.org/10.1016/j.jbiotec.2019.10.022.

30. E. Geiser, M. Reindl, L. M. Blank, M. Feldbrügge, N. Wierckx, and K. Schipper, "Activating Intrinsic Carbohydrate-Active Enzymes of the Smut Fungus *Ustilago maydis* for the Degradation of Plant Cell Wall Components," *Applied and Environmental Microbiology* 82, no. 17 (2016): 5174–5185, https://doi.org/10.1128/AEM.00713-16.

31. S. Robertz, M. Philipp, K. Schipper, et al., "Monitoring Corn Stover Processing by the Fungus *Ustilago Maydis*," *Bioresources and Bioprocessing* 11, no. 1 (2024): 87, https://doi.org/10.1186/s40643-024-00802-3.

32. P. Richter, J. Panchalingam, K. Miebach, K. Schipper, M. Feldbrügge, and M. Mann, "Studying Microbial Triglyceride Production From Corn Stover Saccharides Unveils Insights Into the Galactose Metabolism of *Ustilago maydis*," *Microbial Cell Factories* 23, no. 1 (2024): 204, https://doi.org/10.1186/s12934-024-02483-1.

33. L. Romero-Aguilar, M. Montero-Lomeli, J. P. Pardo, and G. Guerra-Sánchez, "Lipid Index Determination by Liquid Fluorescence Recovery in the Fungal Pathogen *Ustilago Maydis*," *Journal of Visualized Experiments* no. 134 (2018), https://doi.org/10.3791/57279.

34. J.-M. Nicaud, et al., Protocols for Monitoring Growth and Lipid Accumulation in Oleaginous Yeasts, in *Hydrocarbon and Lipid Microbiology Protocols: Bioproducts, Biofuels, Biocatalysts and Facilitating Tools*, eds. T. J. McGenity, K. N. Timmis, and B. Nogales (Springer Berlin Heidelberg, 2017), 153–169.

35. S. Hewald, K. Josephs, and M. Bölker, "Genetic Analysis of Biosurfactant Production in *Ustilago maydis*," *Applied and Environmental Microbiology* 71, no. 6 (2005): 3033–3040, https://doi.org/10.1128/AEM.71.6.3033-3040.2005.

36. C. W. Basse, S. Stumpferl, and R. Kahmann, "Characterization of a *Ustilago Maydis* Gene Specifically Induced During the Biotrophic Phase: Evidence for Negative as Well as Positive Regulation," *Molecular and Cellular Biology* 20, no. 1 (2000): 329–339, https://doi.org/10.1128/MCB.20.1.329-339.2000.

37. R. Holliday, "*Ustilago maydis*," in *Handbook of Genetics*, Vol. 1, ed. R. C. King (Plenum, 1974), 575–595.

38. C. Verduyn, E. Postma, W. A. Scheffers, and J. P. Van Dijken, "Effect of Benzoic Acid on Metabolic Fluxes in Yeasts: A Continuous-Culture Study on the Regulation of Respiration and Alcoholic Fermentation," *Yeast* 8, no. 7 (1992): 501–517, https://doi.org/10.1002/yea.320080703.

39. J. Schindelin, I. Arganda-Carreras, E. Frise, et al., "Fiji: An Open-Source Platform for Biological-Image Analysis," *Nature Methods*, 9, no. 7 (2012): 676–682, https://doi.org/10.1038/nmeth.2019.

40. W. Fei, G. Shui, and B. Gaeta, et al., "Fld1p, a Functional Homologue of Human Seipin, Regulates the Size of Lipid Droplets in Yeast," *Journal of Cell Biology* 180, no. 3 (2008): 473–482, https://doi.org/10.1083/jcb.200711136.

41. S. C. Guimaraes, M. Schuster, and E. Bielska, et al., "Peroxisomes, Lipid Droplets, and Endoplasmic Reticulum 'Hitchhike' on Motile Early Endosomes," *Journal of Cell Biology* 211, no. 5 (2015): 945–954, https://doi.org/10.1083/jcb.201505086.

42. E. Geiser, S. K. Przybilla, and A. Friedrich, et al., "*Ustilago maydis* Produces Itaconic acid Via the Unusual Intermediate Trans-Aconitate," *Microbial Biotechnology* 9, no. 1 (2016): 116–126, https://doi.org/10.1111/1751-7915.12329.

43. B. Teichmann, U. Linne, S. Hewald, M. A. Marahiel, and M. Bölker, "A Biosynthetic Gene Cluster for a Secreted Cellobiose Lipid With Antifungal Activity From *Ustilago maydis*," *Molecular Microbiology* 66, no. 2 (2007): 525–533, https://doi.org/10.1111/j.1365-2958.2007.05941.x.

44. S. Hewald, U. Linne, M. Scherer, M. A. Marahiel, J. Kämper, and M. Bölker, "Identification of a Gene Cluster for Biosynthesis of Mannosylerythritol Lipids in the Basidiomycetous Fungus *Ustilago maydis*," *Applied and Environmental Microbiology* 72, no. 8 (2006): 5469–5477, https://doi.org/10.1128/AEM.00506-06.

45. V. Choudhary, G. Golani, and A. S. Joshi, et al., "Architecture of Lipid Droplets in Endoplasmic Reticulum Is Determined by Phospholipid Intrinsic Curvature," *Current Biology* 28, no. 6 (2018): 915–926.e9, https://doi.org/10.1016/j.cub.2018.02.020.

46. K. Müntjes, M. Philipp, L. Hüsemann, et al., "Establishing Polycistronic Expression in the Model Microorganism *Ustilago maydis*," *Frontiers in Microbiology* 11 (2020): 1384.

47. W.-K. Huh, J. V. Falvo, and L. C. Gerke, et al., "Global Analysis of Protein Localization in Budding Yeast," *Nature* 425 (2003): 686–691, https://doi.org/10.1038/nature02026.

48. J. Zhu, Z.-T. Zhang, and S.-W. Tang, et al., "A Validated Set of Fluorescent-Protein-Based Markers for Major Organelles in Yeast (*Sac-*

charomyces cerevisiae)," *MBio* 10, no. 5 (2019): e01691–19, https://doi.org/10.1128/mbio.01691-19.

49. K.-L. Li and A. E. Humphrey, "Use of Fluorometry for Monitoring and Control of a Bioreactor," *Biotechnology and Bioengineering* 37, no. 11 (1991): 1043–1049, https://doi.org/10.1002/bit.260371109.

50. T. K. Karakach, A. Dachon, J. Choi, C. Miguez, L. Masson, and B. Tartakovsky, "Fluorescence-Based Real Time Monitoring and Diagnostics of Recombinant *Pichia pastoris* Cultivations In A Bioreactor," *Biotechnology Progress* 35, no. 2 (2019): e2761, https://doi.org/10.1002/btpr.2761.

51. H. L. Weil, K. Schneider, M. Tschöpe, et al., "PLANTdataHUB: A Collaborative Platform for Continuous FAIR Data Sharing in Plant Research," *The Plant Journal* 116, no. 4 (2023): 974–988. Portico, https://doi.org/10.1111/tpj.16474.

Supporting Information

Additional supporting information can be found online in the Supporting Information section.

Supporting File 1: elsc70053-sup-0001-SuppMat.pdf.